IR THERMAL WAVE TOMOGRAPHIC STUDIES OF STRUCTURAL COMPOSITES

L.D. Favro, H.J. Jin, Y.X. Wang, T. Ahmed, X. Wang,
P.K. Kuo, and R.L. Thomas

Department of Physics and Institute for Manufacturing Research
Wayne State University, Detroit, MI 48202

INTRODUCTION

Vavilov et al [1] have recently described a technique for making tomographic thermal wave images. Their method involves recording a succession of thermal wave images after a flash-heating pulse, followed by a numerical pixel-by-pixel search of the images for the time at which the reflected thermal waves from subsurface features have their peak amplitudes. Since the peak time is related to the depth of the scatterer, this information enables one to separate the image into time (or depth) slices. The result is a thermal wave tomogram. Since their process involves post-processing and a search through a large number of stored images, it is memory-intensive, and is difficult to accomplish in real time. In the present paper, we report a thermal wave tomographic method which accomplishes the same result, but does so with real-time techniques which avoid the storage of a large number of images, and produces the tomogram without post-processing.

DESCRIPTION OF THE TECHNIQUE

The tomographic method we describe is based on wide area pulse heating (e.g. by flashlamps) of the sample's surface. Experimental curves showing the time dependence of the surface temperature of a sample following such pulse heating are shown in Fig. 1. These curves result from temperature measurements over several subsurface flat bottom holes at different depths in a polymer test specimen, and are plotted together with a curve of the temperature at a point above a featureless region of the same sample. It can be seen that, after the flash occurs, the surface temperature in all regions rises very rapidly to a peak which is essentially independent of spatial position. This is followed by a more or less exponential decay, with the rate of decay varying both in time, and from point to point on the surface. This can be explained in the following way. A typical cooling curve corresponding to some point on the surface can be thought of as being comprised of two components. One component is simply that which would occur if the material underneath that region contained no thermal wave scatterers. The other component results from the thermal wave reflected from any such scatterer. This reflected thermal wave slows the rate of cooling. It can be seen from Fig 1 that there are varying cooling rates over different regions, as expected on the basis of the description above. As mentioned above, the curve with the fastest cooling rate corresponds to the featureless region beneath which there are no subsurface scatterers. In our tomographic method we make use of this curve as a reference and subtract this reference from the time dependence of every pixel of the image as it is generated. Examples of such subtracted curves (expanded in scale) are shown in Fig. 2 for the six selected regions corresponding to the cooling curves of Fig. 1. Because these curves have had the background curve subtracted, they correspond to the arrival back at the surface of the reflected thermal waves from the subsurface holes. Although the peaks are broadened because of the diffusive nature of the heat propagation, the peaks of the subtracted curves

Review of Progress in Quantitative Nondestructive Evaluation, Vol. 11
Edited by D.O. Thompson and D.E. Chimenti, Plenum Press, New York, 1992

(see Fig. 2) are seen to vary both in height and in temporal position, with the peaks corresponding to the deeper holes being lower and later. In our real-time method, we carry out a pixel-by-pixel determination of the peaks of these subtracted curves. This is accomplished by smoothing the curves to avoid spurious peaks caused by noise in the signal, followed by a determination of the peak of the smoothed curve. The resulting 512 x 480 collection of peak times is stored as a pseudo-image in a buffer of the real-time processor. Thus, when the heating and cooling cycle is completed, a real-time tomogram is available in the buffer for viewing. In addition, a second buffer contains a "peak contrast" image. This second image displays each individual pixel as it appeared at the time when its contrast with the background of the image was maximum. Currently, we have the ability to produce both tomographic and peak contrast images simultaneously with a single heating flash, and with post-heating sampling rates up to 10 Hz.

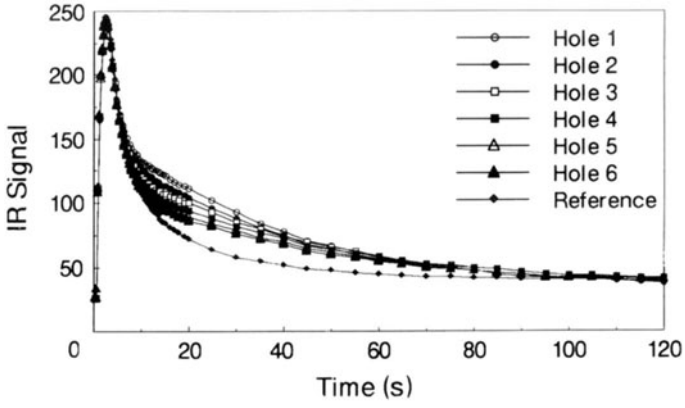

Fig. 1 Heating and cooling curves over six subsurface flat bottom holes at different depths in a plastic sample. The reference (lowest) curve corresponds to a region away from the holes.

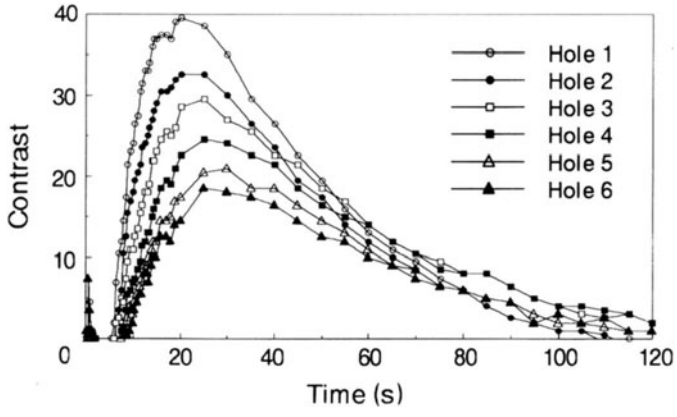

Fig. 2 Subtracted curves (expanded in scale) for the reference curve subtracted from the six curves above the subsurface holes of Fig. 1.

RESULTS

In Fig. 3 we show a tomogram of a graphite-epoxy sample which had been subjected to an impact which caused damage which extends from directly under the point of impact out to the edges of the sample in the horizontal direction. The sample was viewed from the side opposite the impact. The tomogram is displayed with a gray-scale color map for which black represents short time and white represents long time. Figure 3 shows that the damage near the edges is further from the surface than the damage under the impact site. In addition, there are other areas of the sample which indicate reflections from intermediate depths (various levels of gray) which may indicate porosity or incomplete bonding of the plies. Fig. 4 is a peak contrast image of the sample shown in Fig. 3. This image shows each pixel of the image as it appeared when its contrast was maximum. The greatest contrast (white) corresponds to the shallowest defects (compare with Fig. 3), as expected for heat diffusion.

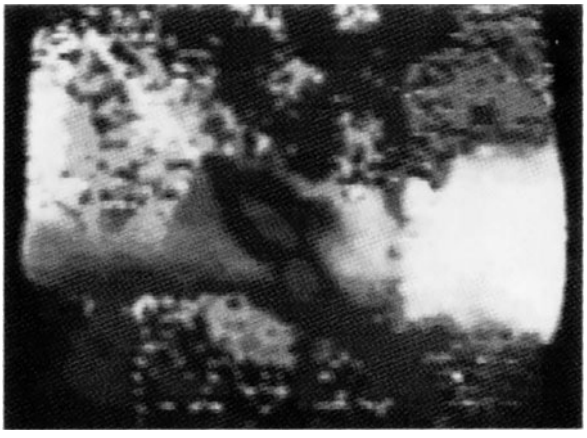

Fig. 3 Thermal wave tomogram of a sample of graphite-epoxy material with impact damage. White indicates longer time (greater depth), black shorter time (lesser depth).

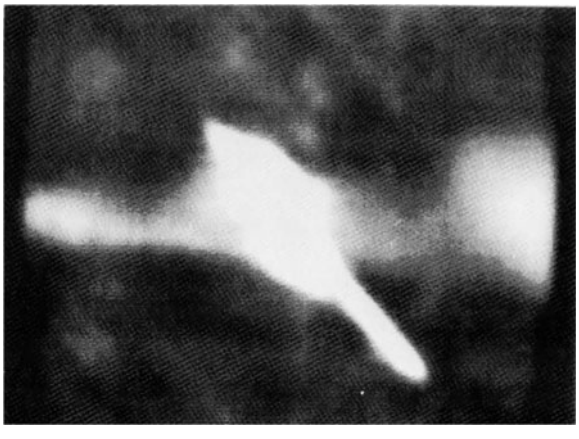

Fig. 4 Peak contrast image of the impact damage sample shown in Fig. 3. White indicates greater contrast, black lesser contrast.

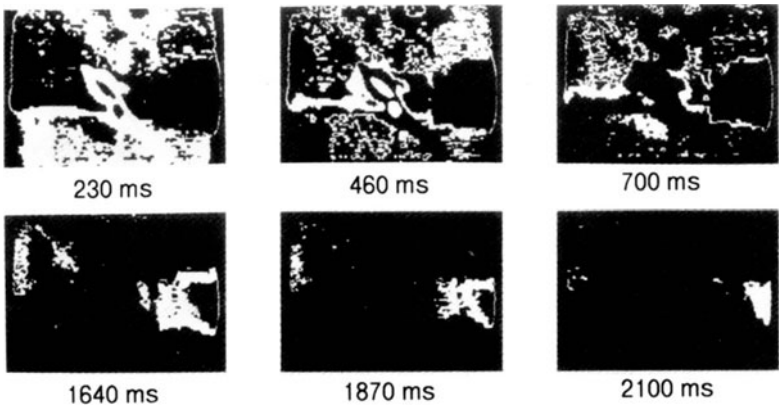

Fig. 5 Time-slice images derived from the tomogram of Fig.3, showing only those features(as white) whose contrast peaks at the times shown beneath each image.

Figure 5 shows a series of time-slice images derived from the tomogram of Fig.3, showing only those features(as white) whose contrast peaks at the times shown beneath each image. At the shortest time (230 ms) following the heating pulse, the features show the pattern of the near-surface fibers, along with a shallow region of delamination surrounding the central feature. At 460 ms, these shallow features begin to fade, and a slightly deeper region of delamination appears beneath the central feature. Next (700 ms), these central features all fade away, and a delamination near the left horizontal edge appears. Finally (1640 ms, 1870 ms, 2100 ms), only the deep delamination near the right edge is seen.

In Fig. 6 we show another sample of impact damage in a graphite-epoxy specimen. This sample is viewed from the impact side and the data are presented as a color perspective plot with greater time plotted downward to give the subjective impression of depth in the image.

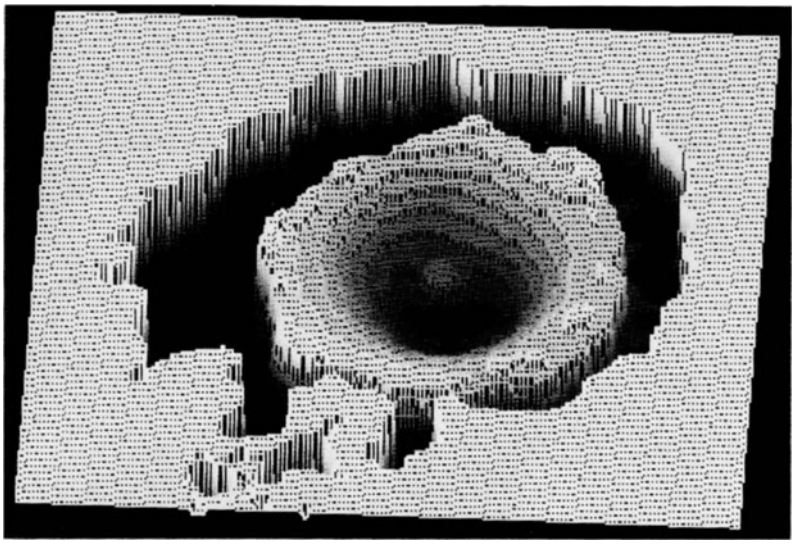

Fig. 6 A tomogram of a second graphite-epoxy impact damage specimen, shown as a perspective plot. Increasing time (depth) is plotted downward.

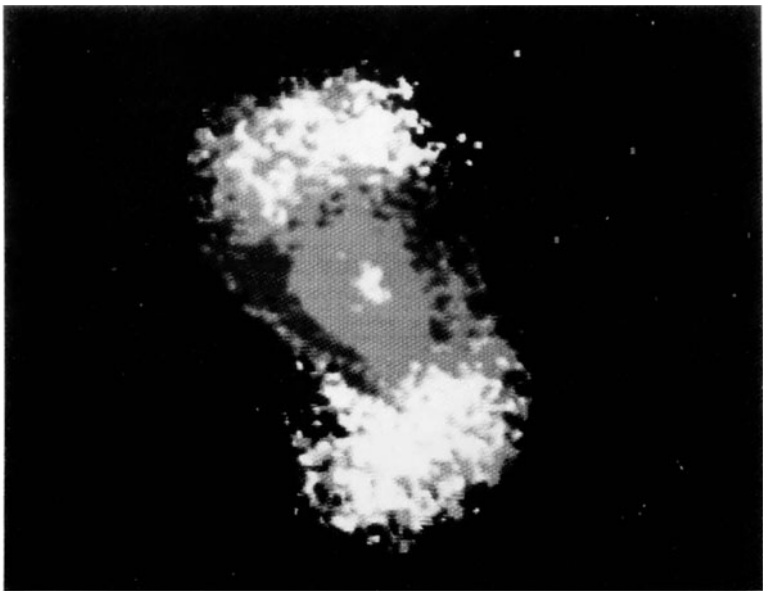

Fig. 7 A tomogram of a third graphite-epoxy sample showing impact damage which spirals to the right as the depth increases.

This impact caused shallow damage directly under and immediately surrounding the point of impact, with a wider ring of much deeper damage caused when the shock wave from the impact neared the rear surface. A final impact damage specimen is shown in Fig. 7. The damage in this specimen tends to spiral to the right as it goes deeper. This presumably results from the rotation of the fiber direction in the deeper plies.

CONCLUSIONS

We have demonstrated a real-time thermal wave IR tomographic method which shows promise for defect depth determinations. The technique has been illustrated by forming tomographic images of impact damage in polymer composite test specimens, which together with the complementary peak contrast images, permits more rapid and quantitative characterization of subsurface damage zones in these materials.

ACKNOWLEDGEMENTS

This work was sponsored by ARO under Contract No. DAAL03-88-K-0089; by the Center for Advanced Nondestructive Evaluation, operated by the Ames Laboratory, USDOE, for the Air Force Wright Aeronautical Laboratories under Contract No. W-7405-ENG-82 with Iowa State University; and by the Institute for Manufacturing Research, Wayne State University.

REFERENCE

1. V. Vavilov, T. Ahmed, H.J. Jin, R.L. Thomas and L.D. Favro, Sov. J. NDT 12 (1990).